Shape-dependence of Pd Nanocrystal Carburization during Acetylene Hydrogenation

Micaela Crespo-Quesada[†,#], *Songhak Yoon*[‡], *Mingshang Jin*[§], *Antonio Prestianni*[|], *Remedios Cortese*[|], *Fernando Cárdenas-Lizana*[†,≡], *Dario Duca*[|], *Anke Weidenkaff*[‡] *and Lioubov Kiwi-Minsker*[*,†]

[†]Group of Catalytic Reaction Engineering, Ecole Polytechnique Fédérale de Lausanne (EPFL), 1015 Lausanne, Switzerland.

[‡]Laboratory for Solid State Chemistry and Catalysis, Swiss Federal Laboratories for Materials Science and Technology (EMPA), 8600 Dübendorf, Switzerland.

[§]Center for Materials Chemistry, Frontier Institute of Science and Technology, Xi'an Jiaotong University, 710054 Xi'an, Shaanxi, People's Republic of China.

[|] Dipartimento di Fisica e Chimica dell'Università degli Studi di Palermo, 90128 Palermo, Italy.

ABSTRACT

This interdisciplinary work combines the use of shape and size-defined Pd nanocrystals (cubes of 10 and 18 nm, and octahedra of 37 nm) with *in situ* techniques and DFT calculations to unravel the dynamic phenomena with respect to Pd reconstruction taking place during acetylene hydrogenation. Notably, it was found that the reacting Pd surface evolved at a different pace depending on the shape of the Pd nanocrystals due to their specific propensity to form carbides under reaction conditions. Indeed, Pd cubes (Pd(100)) reacted with acetylene to form a $PdC_{0.13}$ phase at a rate roughly 6-fold higher than octahedra (Pd(111)), resulting in nanocrystals with different degrees of carburization. DFT calculations revealed changes in the electronic and geometric properties of the Pd nanocrystals imposed by the progressive addition of carbon in its lattice.

Keywords: palladium carbide, structure sensitivity, XRD, DFT, surface rearrangement.

INTRODUCTION

Alkyne hydrogenations are fundamental reactions in the manufacture of fine and industrial chemicals.[1] While many metals have been found to catalyze the full hydrogenation of alkynes under mild conditions, Pd is widely considered as the best-performing catalyst in terms of alkene yield.[2] Selective acetylene hydrogenation to ethylene is a key step in the production of polyethylene because polymer-grade ethylene tolerates extremely low quantities of the former (*ca*. 5 ppm).[3]

The morphology (shape and size) of the active Pd nanocrystals has a great impact on their catalytic performance in alkyne hydrogenations.[4,5] When a dependence of activity, expressed as turnover frequency (TOF), with particle morphology can be established, the reaction is then referred to as structure-sensitive. Much effort has been devoted to the investigation of the structure sensitivity of acetylene hydrogenation.[6-8] Most studies deal with the effects of particle size,[9] and have found that the reaction shows antipathetic structure sensitivity, *i.e*. the TOF increases with increasing particle size.[8,10-12] The effects of shape, on the other hand, have been far less addressed. Although there are several theoretical studies of acetylene hydrogenation over single planes,[9,13] there is only a handful of experimental results dealing with real catalysts, where the TOF was found to depend on the crystallographic plane exposed, showing activities of Pd(111) > Pd(100),[12] or correlating the catalytic response to the number of crystal boundaries present in a Pd nanowire.[14]

Particle morphology is not the only factor affecting the catalytic response. Indeed, the surface chemistry of the metal nanoparticle can be drastically altered by the reacting molecules[15,16] and the by-products formed. Palladium can readily form hydrides[15,17-20] in the presence of hydrogen, which have been reported to favor the full hydrogenation to the alkane.[21] On the other hand, the

formation of a Pd carbide phase (PdC_x) in the early stages of the reaction has been widely documented[16,19,20,22,23]. Recent studies performed with *in situ* (mostly under ultra-high vacuum, conditions) techniques such as XPS,[16,22-25] XRD,[26,27] XANES,[19,28] PGGA[16] and EXAFS,[28] and DFT calculations[14,21,25] have shown that PdC_x is formed homogeneously throughout the entire Pd nanoparticle starting from the surface,[28] and then propagates into the bulk. The experimental work performed either on single crystals or with model catalysts, as well as the DFT calculations revealed that the formation of PdC_x is itself a *structure sensitive* phenomenon. Teschner and co-workers[23] experimentally showed that Pd(111) resisted the formation of PdC_x, (confirmed also by DFT calculations), but Pd(100) revealed a strong thermodynamic driving force towards acetylene decomposition and subsequent PdC_x formation.[25]

In this work, the dynamics of PdH and PdC_x formation was studied via *in situ* XRD under technologically relevant conditions. DFT calculations of the acetylene adsorption on Pd(111) and Pd(100) planes were performed in order to gain insight into the carburization phenomenon. The performance of catalysts is often assessed on size-controlled (and more rarely shape-controlled) nanocrystals at initial conditions, where surface modification and deactivation has not yet taken place. These results are used to draw conclusions on the structure sensitivity of the reaction. However, here we show that the surface of the catalysts, and thus their catalytic performance should change with time as a result of atomic rearrangements occurring in the Pd nanocrystals through the interaction with the reacting molecules. This phenomenon is here shown to depend on nanocrystal morphology, and therefore, the observed structure sensitivity of acetylene hydrogenation may be a result of this surface rearrangement.

EXPERIMENTAL AND COMPUTATIONAL METHODS

Preparation of nanocrystals. The Pd nanocubes were synthesized according to our previously published protocols.[29,30] In a typical synthesis, 11 mL of an aqueous solution containing poly(vinyl pyrrolidone) (PVP, MW ≈ 55,000, 105 mg, Aldrich), L-ascorbic acid (60 mg, Aldrich), KBr (300 mg for 10-nm nanocubes and 600 mg for 18-nm nanocubes, Fisher), and sodium tetrachloropalladate (Na_2PdCl_4, 57 mg, Aldrich) was heated at 80 ºC in air under magnetic stirring for 3 h. The Pd octahedra were prepared as reported in our previous protocol.[31] In a typical procedure, 3 mL of aqueous Na_2PdCl_4 solution (32 mM) was introduced into 8 mL of an aqueous solution containing 105 mg PVP, 100 μL HCHO, and 0.3 mL of an aqueous suspension (1.8 mg/mL in concentration) of Pd cubic seeds 18 nm in edge length, which had been heated at 60 ºC for 5 min under magnetic stirring in a capped vial. The reaction was then allowed to proceed at 60 ºC for 3 h. The final products were collected by centrifugation and washed with ethanol and water to remove excess PVP. The nanocrystals were subsequently immobilized on commercially available SiO_2 (S5505, Sigma-Aldrich) by wet impregnation.

Characterization techniques. The shape and size of the nanocrystals were analysed by transmission electron microscopy (TEM), using a Philips CM12 microscope operated at 120 kV.

To determine the amount of Pd in each catalyst, an aliquot of the nanoparticle suspension was analysed by atomic absorption spectroscopy (AAS, Shimadzu AA-6650). The specific wavelength used for Pd^{2+} was 475 nm.

In situ powder XRD patterns were obtained using a PANalytical X´Pert PRO θ-θ scan system with Cu-K_α radiation (λ = 1.5418 Å). The diffraction patterns were recorded with an angular step of 0.05˚. The powder samples were placed in the heating chamber (XRK 900, Anton Paar) and gas was applied through the mass flow controller (5850 TR, Brooks instrument). The used gas

were N_2 (99.999%, Messer), H_2 (99.999%, Messer and C_2H_2 (> 99.5%, PanGas). Roughly 0.03 g of sample powders was heated under N_2 flow (cm^3 min^{-1}) up to 373 K or 423 K with a heating rate of 10 K min^{-1}. Peak fitting was performed using the software *Fityk*[32] .

Surface area and Pd dispersion were determined via CO chemisorption using Micromeritics (Autochem II 2920). The samples were loaded into a U-shaped quartz cell (3.76 mm i.d.), heated in 20 cm^3 min^{-1} 2% H_2/He at 10 K min^{-1} to 373 K and held for 15 min. The samples were subsequently out gassed in Ar at 373 K for 30 min after which the temperature was decreased to ambient conditions. The CO-chemisorption experiments were performed at 323 K using He as carrier gas. A 3% CO/He mixture gas was pulsed through the sample until the peaks were equal. In a series of blank tests, chemisorption measurements on SiO_2 did not result in any detectable uptake.

Computational details. The calculations of the acetylene adsorption on Pd_{36} and $Pd_{36}C_n$ cluster models (with n=1, 2, 6) were performed using *Gaussian 09*.[33] The hybrid Becke's three parameters exchange-correlation functional B3LYP was used throughout.[34] Los Alamos LANL2 pseudopotential and the corresponding valence basis set[35] were used for Pd atoms, while the LANL2dp with polarization functions basis set was employed for C and H atoms. The starting structure for Pd_{36} cluster was obtained using a fragment extracted from one Pd *fcc* bulk structure (space group *Fm-3m*, a = 3.879 Å). It was subjected to full geometry optimization and the nature of the optimized structures was defined by inspection of the harmonic vibrational frequencies. All the energy values were corrected for the zero-point vibrational contribution. Interaction energies were computed as $\Delta E = E_{acetylene/Pd36} - (E_{Pd36} + E_{acetylene})$; thus, negative values correspond to the formation of stable aggregates. In order to assess the reliability of the cluster models above, periodic calculations were also performed both on (111) and (100) Pd surfaces. The

reference periodic models were formed by adsorbed acetylene molecules on Pd surfaces belonging to unit cells singly formed either by just palladium atoms (bare system) or by palladium embedding carbon atoms placed in subsurface layers, having a whole atomic ratio C:Pd = 1:45 (carburized system). These calculations were performed using the SIESTA[36] method applied on a p(3x3) unit cell with a thickness of six layers. Careful benchmarks were carried out in order to select adequate values both for the k-space sampling (10x10x1) and for the sharpness of the real space grid (500 Ry). Troullier-Martins pseudopotentials for H, C and Pd were generated and tested. For Pd non-linear core correction were also included. Customized basis sets were built up for all the atoms, in the case of Pd an appropriate extent of the numerical atomic orbitals was guaranteed in order to describe properly the vacuum region at the interface. As exchange-correlation functional the DRSLL parameterization[37] of the vdW-DF functional was selected.

RESULTS AND DISCUSSION

Well-defined Pd nanocrystals supported on SiO_2. TEM images of the as-prepared nanocrystals *i.e*. cubes of 10 nm (CUBA) and 18 nm (CUBB) in edge length and enclosed mainly by Pd(100) atoms, and octahedra of 37 nm (OCT) in edge length and enclosed mainly by Pd(111) atoms, can be found in Figure 1, panels ia, ib and ic. Panels iia, iib and iic in Figure 1 show TEM pictures of the fresh nanocrystals immobilized on commercial SiO_2, thus obtaining 1.8, 5.0 and 3.6 wt.% Pd loading in the final catalysts, respectively.

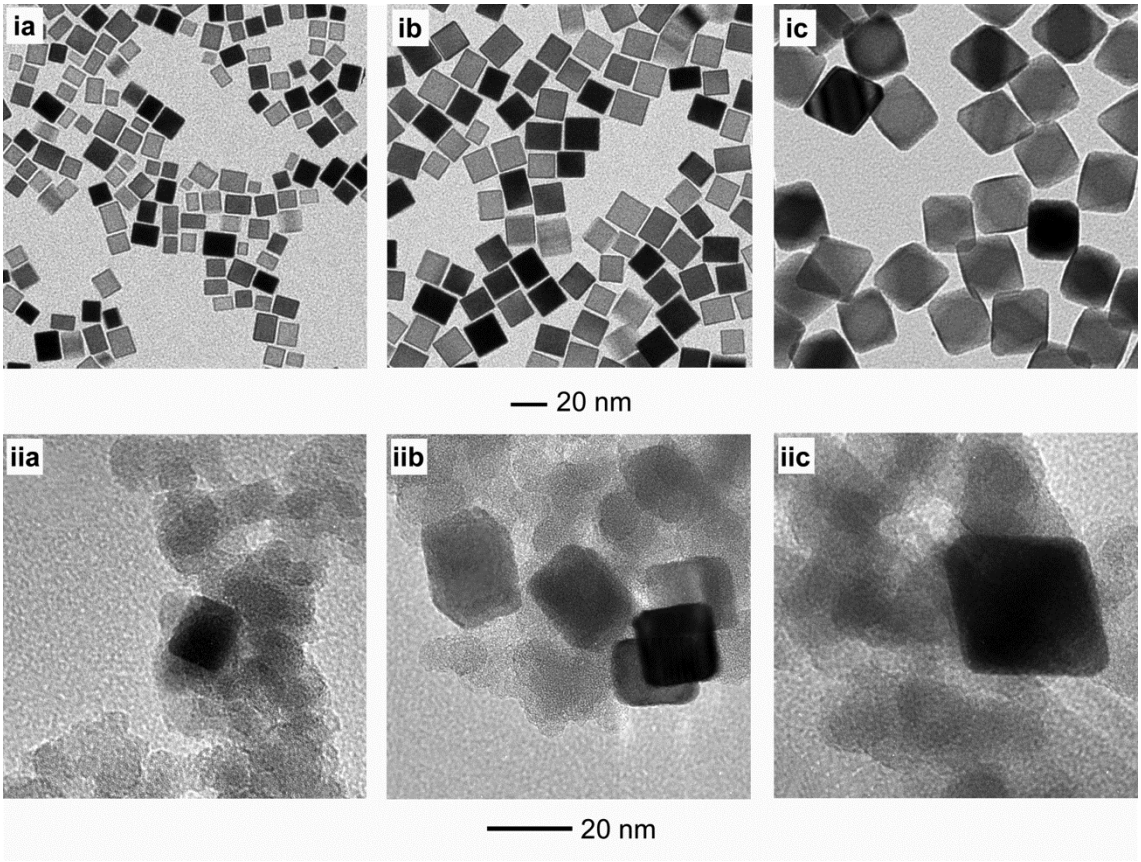

Figure 1. TEM images of i) unsupported and ii) SiO_2-supported Pd nanocrystals: a) 10-nm cubes (CUB_A), b) 18-nm cubes (CUB_B), and c) 37-nm octahedra (OCT).

It can be appreciated that the shape of the nanocrystals is not altered during immobilization. Table 1 shows the main characteristics of the catalysts. The highly loaded CUB_B/SiO_2 and OCT/SiO_2 catalysts present lower Pd dispersions probably due to some agglomeration.

Table 1. Catalyst characteristics

Catalyst	Surface characteristics				
	wt. Pd [%]	d_{nc} [nm]	D_{est} [a] [%]	D_{exp} [b] [%]	$S_{Pd,exp}$ [b] [$m^2\ g^{-1}$]
CUB_A/SiO_2	1.8	10	8.8	7.5	33.5
CUB_B/SiO_2	5.0	18	5.0	2.3	10.4
OCT/SiO_2	3.6	37	2.8	2.3	10.3

[a]The dispersion was estimated based on the surface statistics of *fcc* crystals[51] assuming one face of the nanocrystal was unavailable due to the interaction with the support.

[b]Determined by CO-chemisorption.

The dynamics and structure sensitivity of PdCx formation. Amongst the wealth of publications revolving around the formation of PdC_x during reactions, there is only a handful dealing with its characterization under technologically relevant conditions, especially over well-defined nanocrystals.[19,28] Even in those cases, little information was given concerning the morphology of the active phase. This probably arises from the fact that only recent advances in nanotechnology has allowed to control the size and shape of metallic nanocrystals and to apply this knowledge to the service of catalysis.[38]

Time-resolved patterns of the catalysts acquired during pretreatment and reaction at ambient pressure obtained by *in situ* XRD are plotted in Figure 2. Panels ia, ib and ic show the evolution of the Pd and PdC_x phases during the entire experiment, whereas panels iia, iib and iic

correspond to 2D projections during acetylene hydrogenation. The detailed experimental procedure can be found in the Supporting Information (SI), Table S1.

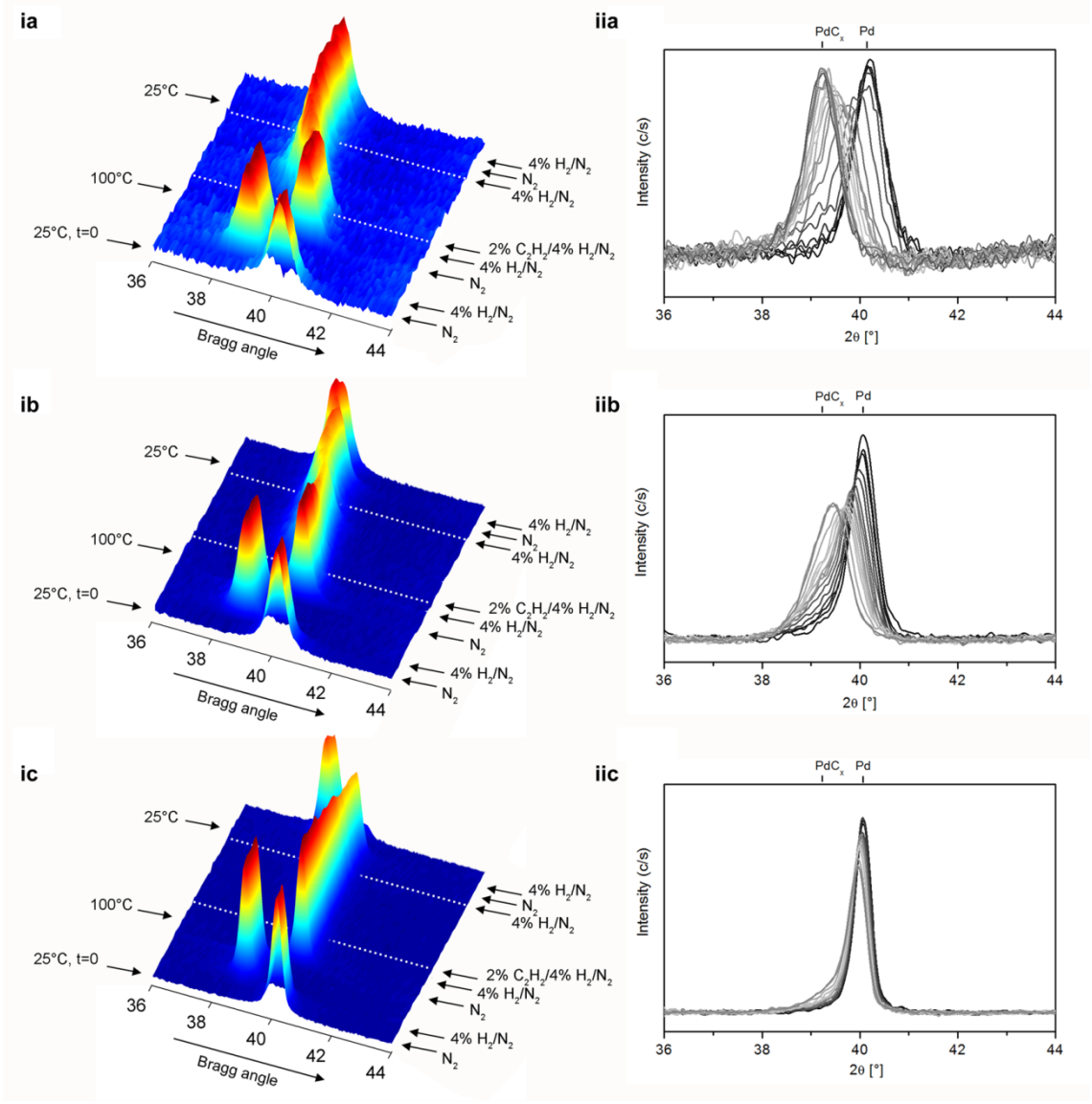

Figure 2. i) Time-resolved XRD analysis performed on the supported Pd nanocrystals; ii) XRD patterns recorded between the dotted lines represented in two dimensions of a) CUB_A/SiO_2, b) CUB_B/SiO_2 and c) OCT/SiO_2 under various conditions.

The initial spectrum of the catalysts under N_2 at room temperature corresponds to the (111) reflection of metallic Pd (40.2° in 2θ, JCPDS-ICDD reference 46-1043). When the samples were

subjected to a flow of 100 mL min^{-1} 4% H_2 in N_2 at room temperature, the reflection shifted almost instantaneously from 40.2° to 38.8° for all samples, being consistent with the reported formation of PdH.[17] This phenomenon was found to be reversible at room temperature, since switching back to an inert gas flow displaced the reflection back to its original position, which concurs with data available in the literature.[18] All samples were subsequently heated up to 373 K under N_2 and subjected once again to a 4% H_2 in N_2 flow for 30 min but no reflection shift was observed in this case, in line with previous findings showing the decomposition of the PdH phase at temperatures ≥343 K.[39,40] This pretreatment in hydrogen flow ensured not only the metallic state of the Pd nanocrystals before the reaction, but also the absence of the PdH phase, which has been classically deemed responsible for non-selective alkyne hydrogenation.[21]

The gas flow was then switched to the reaction mixture (2% C_2H_2 and 4% H_2 in N_2) and short scans of 3 min were continuously recorded. A clear shift to slightly lower scattering angles (39.1° in 2θ) indicates the full carburization of CUBA/SiO_2.[26] The PdC_x phase is similar to that of PdH, in which the carbide retains the fcc structure of metallic Pd while C occupies the octahedral sites of the Pd lattice.[18,41] The incorporation of C atoms induces the lattice expansion (lattice parameter, a) in proportion to the fraction of guest atoms (x = C/Pd), as expressed by the following equation[41,42]:

$$a = a_0 + 0.69x \text{ (Å)} \quad (1)$$

Therefore, the saturation of Pd in CUBA/SiO_2 (Figure 2 iia) can be calculated to occur at x = 0.13, in good agreement with the maximum carbon uptake reported in the literature.[18,41-43] Since the shifts of Bragg reflection are proportional to the volumetric phase transformation, CUB_B/SiO_2 (x = 0.09) and OCT/SiO_2 (x = 0.02) samples do not appear to reach full carburization during a period of 3 h. The PdC_x phase was found to be stable at 373 K under N_2 atmosphere. Moreover,

exposure of the samples to 4% H_2 in N_2 after cooling to room temperature under N_2 did not generate the PdH phase for CUB_A/SiO_2, whereas a distinguishable peak shift towards lower scattering angles could be observed for CUB_B/SiO_2 and OCT/SiO_2 evidencing the formation of PdH phase and explicitly suggesting that fully carburized nanocrystals hindered the dissolution of H in the bulk of $PdC_{0.13}$. This concurs with a previous report, where the interplay between PdC_x and H_2 was analyzed by *in situ* XRD showing the possible existence of a ternary PdC_xH_y phase when $x < 0.13$.[26]

In order to evaluate the structure sensitivity of PdC_x formation, the degree of reflection shift was related to the amount of C in the Pd lattice. The results are shown in Figure 3a. Carburization rates (in $mol_C \cdot mol_{Pd}^{-1} \cdot h^{-1}$) were estimated from the slopes of the curves up to x = 0.04, and are shown on Figure 3b. The rates were normalized by the active metallic Pd surface as determined by CO chemisorption (Table 1), giving rise to surface carburization rates (in $mmol_C$ nm_{Pd}^{-2} h^{-1}), presented in Figure 3b. The surface carburization rates show a clear shape dependence: C is incorporated into cubes, and thus Pd(100), 6-fold faster than into octahedra, *i.e.* Pd(111), as has already been found on single crystals[23] and shown via DFT calculations.[25] Concerning size effects, we found that the surface carburization rate on Pd(100) seems to be independent of nanocrystal size (at least for 10 and 18 nm). There is a substantial lack of information concerning the size effects of Pd nanocrystals on carbide formation. Han et al. have suggested, employing *ex situ* XRD, that Pd nanocrystals below 2.4 nm were more resistant to carbide formation than their larger counterparts due to the metal non-metal transition that could lead to drastically altered chemical properties.[44] This does not conflict with our findings and suggests that there is probably a critical size (*ca.* 2.5 nm[44]) above which size does not significantly impact carbide formation. It is worth noting that the morphology of shape-

controlled nanocrystals under similar reaction conditions was not affected as shown in a previous study[45], and therefore, the shape and size of the nanocrystals used in this study is most probably preserved throughout the duration of the *in situ* measurements.

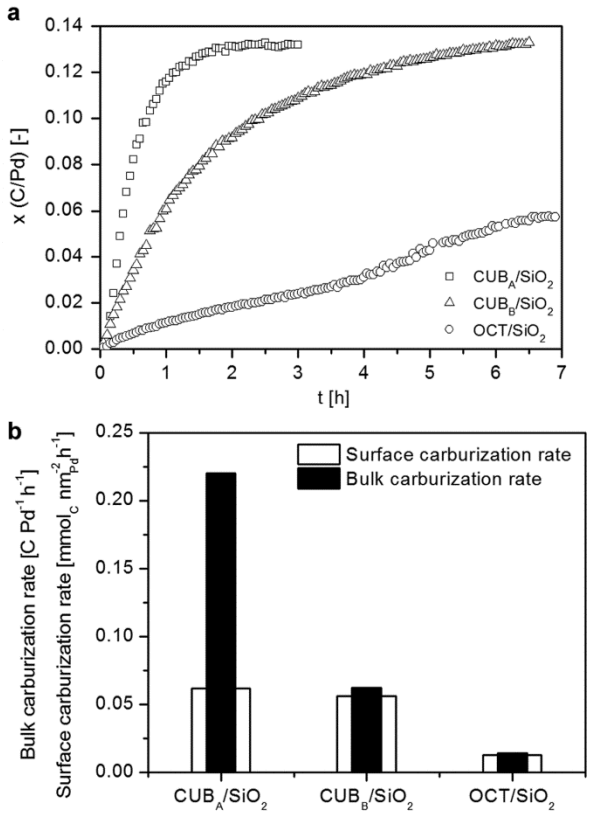

Figure 3. a) Time-resolved incorporation of C into the Pd lattice for CUB_A/SiO_2, CUB_B/SiO_2 and OCT/SiO_2 and b) bulk carburization rate and surface carburization rate of each catalyst (obtained from panel a).

We also studied the influence of different parameters (*e.g.* temperature, acetylene concentration and hydrogen concentration) on the carburization rate. Figure S1, panel a (see SI) shows that an increase in temperature of 50 K tripled the bulk carburization rate of OCT. On the other hand, a change in acetylene concentration did not result in a drastic change of carburization rate (see SI, Figure S2), suggesting that the heat of adsorption is high enough to provide a

maximum coverage even at low concentrations. Finally, hydrogen seems to be necessary to form palladium carbide since the absence of the former almost completely inhibited the formation of the latter. The need of H_2 to form PdC_x has already been observed experimentally.[27] This can be explained by the change in the sticking probability of acetylene when H_2 is co-adsorbed. In the absence of H_2, acetylene converts to vinylidene,[46] whereas in the presence of hydrogen, acetylene hydrogenates to ethylene or ethylidyne probably via vinyl,[47] the former being much less reactive than the latter.[48] On the other hand, when an excess of hydrogen is present in the system, the hydrogenation reaction is probably favored with respect to C-C scission and carbide formation, as was also recently demonstrated by DFT calculations.[49]

In order to better understand this phenomenon, we performed DFT calculations on a Pd_{36} cluster, containing both Pd(111) and Pd(100) faces, and on $Pd_{36}C_n$ derivatives, n being 1, 2, 6. Panels ia, ib, ic and id in Figure 4 show the Pd_{36}, $Pd_{36}C$, $Pd_{36}C_2$ and $Pd_{36}C_6$ models, respectively. The acetylene interaction energies on the Pd(100) and Pd(111) palladium planes both on the bare Pd_{36} cluster or on $Pd_{36}C_n$ derivatives were subsequently obtained (Table 2). Figure 4 iia shows the most stable adsorption configuration of acetylene on the Pd_{36}(100) plane, which was found to occur on a four-fold hollow site. A similar configuration was identified for the $Pd_{36}C_6$ cluster.

It is worth noting that the periodic calculations performed on the Pd surfaces of the bare systems gave results in very good agreement with those obtained with the Pd_{36} model, being as an example the adsorption energy of acetylene on (111) and (100) planes -143.0 and -218.9 kJ mol^{-1} and being the binding sites three- and four-fold hollow, respectively. Also the results concerning the periodic (111) carburized system were in good agreement with those of the carburized cluster model, having the former and the latter adsorption energies equal to -146.0 and -158 kJ mol^{-1}, respectively.

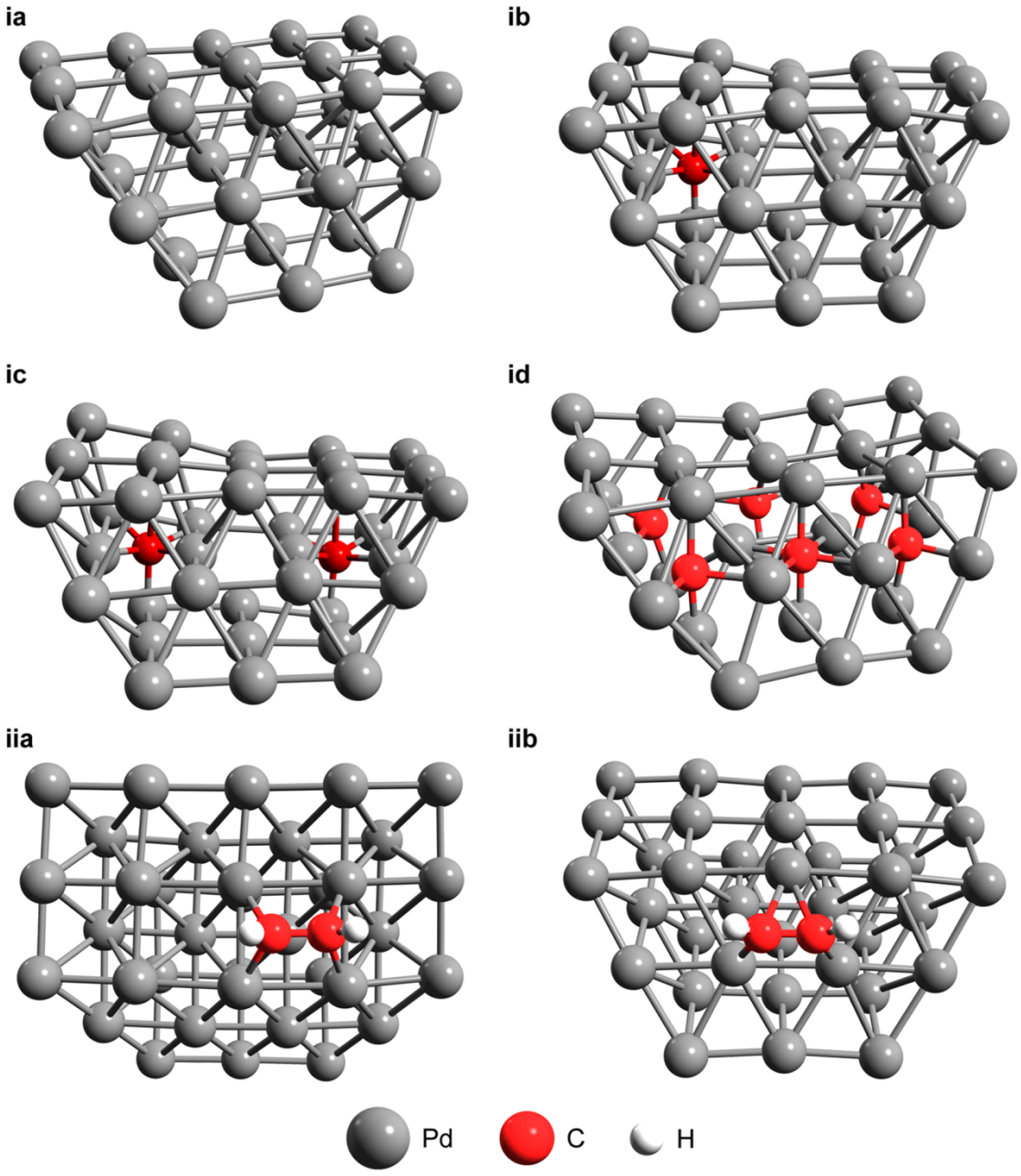

Figure 4. ia) Pd_{36} cluster, ib) $Pd_{36}C$, ic) $Pd_{36}C_2$ and id) $Pd_{36}C_6$ carburized cluster, showing both Pd(100) and Pd(111) Pd planes; ii) C_2H_2/Pd_{36}, representing the most stable adsorption modes on the a) Pd(100) and b) Pd(111) palladium planes, respectively. The adsorption modes on the carburized clusters were similar, showing also for these systems four- and a three-fold hollow sites for the Pd(100) and Pd(111) planes, respectively.

Therefore, it can be inferred that, at least for the title systems, a substantial equivalence exists between the cluster and the periodic calculation approaches here employed. Hence, the results of the former although affected by the intrinsic finiteness of the cluster model seem to be safely usable for describing the effects of the palladium carburization processes, even if experimentally occurring on large metal particles. In particular, the interaction energy of C_2H_2 on Pd(100) was found to decrease with the presence of C, from *ca*. 209 kJ mol^{-1} to *ca*. 129 kJ mol^{-1} for the Pd_{36} and a $Pd_{36}C_6$ systems, respectively. This result is in agreement with the experimental findings, showing a higher carburization rate over Pd(100) with respect to Pd(111). Therefore, it is possible to hypothesize that the first C_2H_2 molecules which get in contact with bare Pd(100) are strongly adsorbed and hence, readily decomposed to C atoms, outright able to diffuse into the metallic lattice. A similar conclusion was drawn from recent DFT calculations on several different surfaces of Pd.[50]

Table 2. Pd lattice characteristics and C_2H_2/Pd interaction energies (ΔE) calculated with DFT

Cluster	Pd lattice		C_2H_2-Pd interaction			
			Pd(100)		Pd(111)	
	Distance Pd-Pd[a] [pm]	Distance Pd-C[a,b] [pm]	ΔE [kJ mol^{-1}]	Distance C-C[c] [pm]	ΔE [kJ mol^{-1}]	Distance C-C[c] [pm]
Pd_{36}	278	-	-209	141	-146	137
$Pd_{36}C$	280	199	-	-	-158	137
$Pd_{36}C_2$	282	200	-	-	-163	137
$Pd_{36}C_6$	288	228	-129	136	-60	133

[a]Average values.
[b]It refers to bulk C.
[c]C-C bond length of adsorbed acetylene.

Combining *in situ* methods and computational tools, we were able to show that the dynamic transformation of the surface of Pd nanocrystals depends on their shape. A complex atomic rearrangement occurs at the onset of the reaction, and the state of the surface for each shape depends on its propensity to adsorb and break the C≡C bond as compared to the C diffusion rate within the Pd fcc lattice. This results in different degrees of carburization on different shapes during the hydrogenation of acetylene, which could in turn be responsible for the observed structure-sensitive phenomena.

CONCLUSIONS

We synthesized size-controlled Pd nanocubes (10 nm and 18 nm) and octahedra (37 nm), supported them on SiO_2 and tested in the hydrogenation of acetylene under technologically relevant conditions (373 K, C_2H_2:H_2:Ar = 2:4:94, P_{amb}) thus closing the material and pressure gaps. The surface chemistry of Pd nanocrystals was studied under reaction conditions via *in situ* XRD. Acetylene reacted differently with (100) and (111) planes to form a $PdC_{0.13}$ phase being roughly 6-fold faster on cubes (Pd(100)) than on octahedra (Pd(111)). DFT calculations ascribed this phenomenon to a stronger interaction of acetylene with Pd(100) which led to the C-C bond scission and C incorporation into the Pd lattice. No effect of Pd particle size was observed within the dimensions studied.

ASSOCIATED CONTENT

Supporting Information Available: Experimental conditions during *in situ* XRD analysis of the catalysts, the effect of temperature, acetylene and hydrogen concentration on carburization rates. This material is available free of charge via the Internet at http://pubs.acs.org.

AUTHOR INFORMATION

Corresponding Author

*lioubov.kiwi-minsker@epfl.ch, +41 (0)21 693 31 82

Present Addresses

[#]Department of Chemistry, University of Cambridge, CB2 1EW Cambridge, UK.

[=]Institute of Mechanical, Process and Energy Engineering (IMPEE), School of Engineering and Physical Sciences (EPS), Heriot-Watt University, EH14 4AS Edinburgh, UK.

ACKNOWLEDGMENTS

The Swiss National Science Foundation (Grant #200021-118067 to LKM) is acknowledged for financial support. YX has been supported by the NSF (DMR-1215034). MJ has been supported by the “start-up fund” and “the Fundamental Research Funds for the Centeral Universities” of Xi’an Jiaotong University.

REFERENCES

1. Blaser, H. U., Heterogeneous Catalysis for Fine Chemicals Production. *Catal. Today* **2000**, 60, 161-165.
2. Chen, B.; Dingerdissen, U.; Krauter, J. G. E.; Rotgerink, H. G. J. L.; Mobus, K.; Ostgard, D. J.; Panster, P.; Riermeier, T. H.; Seebald, S.; Tacke, T., et al., New Developments in Hydrogenation Catalysis Particularly in Synthesis of Fine and Intermediate Chemicals. *Appl. Catal. A-Gen.* **2005**, 280, 17-46.
3. Duca, D.; Arena, F.; Parmaliana, A.; Deganello, G., Hydrogenation of Acetylene in Ethylene Rich Feedstocks: Comparison between Palladium Catalysts Supported on Pumice and Alumina. *Appl. Catal. A-Gen.* **1998**, 172, 207-216.
4. Crespo-Quesada, M.; Cárdenas-Lizana, F.; Dessimoz, A.-L.; Kiwi-Minsker, L., Modern Trends in Catalyst and Process Design for Alkyne Hydrogenations. *ACS Catal.* **2012**, 2, 1773-1786.
5. Crespo-Quesada, M.; Yarulin, A.; Jin, M. S.; Xia, Y. N.; Kiwi-Minsker, L., Structure Sensitivity of Alkynol Hydrogenation on Shape- and Size-Controlled Palladium Nanocrystals: Which Sites Are Most Active and Selective? *J. Am. Chem. Soc.* **2011**, 133, 12787-12794.
6. Borodziński, A., The Effect of Palladium Particle Size on the Kinetics of Hydrogenation of Acetylene-Ethylene Mixtures over Pd/Sio2 Catalysts. *Catal. Lett.* **2001**, 71, 169-175.
7. Ruta, M.; Laurenczy, G.; Dyson, P. J.; Kiwi-Minsker, L., Pd Nanoparticles in a Supported Ionic Liquid Phase: Highly Stable Catalysts for Selective Acetylene Hydrogenation under Continuous-Flow Conditions. *J. Phys. Chem. C* **2008**, 112, 17814-17819.

8. Tribolet, P.; Kiwi-Minsker, L., Palladium on Carbon Nanofibers Grown on Metallic Filters as Novel Structured Catalyst. *Catal. Today* **2005**, 105, 337-343.
9. Duca, D.; Varga, Z.; La Manna, G.; Vidoczy, T., Hydrogenation of Acetylene-Ethylene Mixtures on Pd Catalysts: Study of the Surface Mechanism by Computational Approaches. Metal Dispersion and Catalytic Activity. *Theor. Chem. Acc.* **2000**, 104, 302-311.
10. Che, M.; Bennett, C. O., The Influence of Particle-Size on the Catalytic Properties of Supported Metals. *Adv. Catal.* **1989**, 36, 55-172.
11. Ruta, M.; Semagina, N.; Kiwi-Minsker, L., Monodispersed Pd Nanoparticles for Acetylene Selective Hydrogenation: Particle Size and Support Effects. *J. Phys. Chem. C* **2008**, 112, 13635-13641.
12. Yarulin, A. E.; Crespo-Quesada, R. M.; Egorova, E. V.; Minsker, L. L. K., Structure Sensitivity of Selective Acetylene Hydrogenation over the Catalysts with Shape-Controlled Palladium Nanoparticles. *Kinet. Catal.* **2012**, 53, 253-261.
13. Duca, D.; Barone, G.; Varga, Z., Hydrogenation of Acetylene-Ethylene Mixtures on Pd Catalysts: Computational Study on the Surface Mechanism and on the Influence of the Carbonaceous Deposits. *Catal. Lett.* **2001**, 72, 17-23.
14. He, Y. F.; Feng, J. T.; Du, Y. Y.; Li, D. Q., Controllable Synthesis and Acetylene Hydrogenation Performance of Supported Pd Nanowire and Cuboctahedron Catalysts. *ACS Catal.* **2012**, 2, 1703-1710.
15. Garcia-Mota, M.; Bridier, B.; Perez-Ramirez, J.; Lopez, N., Interplay between Carbon Monoxide, Hydrides, and Carbides in Selective Alkyne Hydrogenation on Palladium. *J. Catal.* **2010**, 273, 92-102.

16. Teschner, D.; Revay, Z.; Borsodi, J.; Havecker, M.; Knop-Gericke, A.; Schlogl, R.; Milroy, D.; Jackson, S. D.; Torres, D.; Sautet, P., Understanding Palladium Hydrogenation Catalysts: When the Nature of the Reactive Molecule Controls the Nature of the Catalyst Active Phase. *Angew. Chem. Int. Edit.* **2008**, 47, 9274-9278.
17. Vogel, W.; He, W.; Huang, Q.-H.; Zou, Z.; Zhang, X.-G.; Yang, H., Palladium Nanoparticles "Breathe" Hydrogen; a Surgical View with X-Ray Diffraction. *Int. J. Hydrogen Energy* **2010**, 35, 8609-8620.
18. Mccaulley, J. A., In-Situ X-Ray-Absorption Spectroscopy Studies of Hydride and Carbide Formation in Supported Palladium Catalysts. *J. Phys. Chem.* **1993**, 97, 10372-10379.
19. Tew, M. W.; Janousch, M.; Huthwelker, T.; van Bokhoven, J. A., The Roles of Carbide and Hydride in Oxide-Supported Palladium Nanoparticles for Alkyne Hydrogenation. *J. Catal.* **2011**, 283, 45-54.
20. Tew, M. W.; Miller, J. T.; van Bokhoven, J. A., Particle Size Effect of Hydride Formation and Surface Hydrogen Adsorption of Nanosized Palladium Catalysts: L-3 Edge Vs K Edge X-Ray Absorption Spectroscopy. *J. Phys. Chem. C* **2009**, 113, 15140-15147.
21. Doyle, A. M.; Shaikhutdinov, S. K.; Jackson, S. D.; Freund, H. J., Hydrogenation on Metal Surfaces: Why Are Nanoparticles More Active Than Single Crystals? *Angew. Chem. Int. Edit.* **2003**, 42, 5240-5243.
22. Teschner, D.; Borsodi, J.; Wootsch, A.; Révay, Z.; Hävecker, M.; Knop-Gericke, A.; Jackson, S. D.; Schlögl, R., The Roles of Subsurface Carbon and Hydrogen in Palladium-Catalyzed Alkyne Hydrogenation. *Science* **2008**, 320, 86-89.

23. Teschner, D.; Vass, E.; Havecker, M.; Zafeiratos, S.; Schnorch, P.; Sauer, H.; Knop-Gericke, A.; Schloegl, R.; Chamam, M.; Wootsch, A., et al., Alkyne Hydrogenation over Pd Catalysts: A New Paradigm. *J. Catal.* **2006**, 242, 26-37.
24. Vass, E. M.; Havecker, M.; Zafeiratos, S.; Teschner, D.; Knop-Gericke, A.; Schlogl, R., The Role of Carbon Species in Heterogeneous Catalytic Processes: An in Situ Soft X-Ray Photoelectron Spectroscopy Study. *J. Phys.-Condens. Mat.* **2008**, 20.
25. Seriani, N.; Mittendorfer, F.; Kresse, G., Carbon in Palladium Catalysts: A Metastable Carbide. *J. Chem. Phys* **2010**, 132.
26. Vogel, W., Interaction of a Nanosized Pd Catalyst with Active C from the Carbon Support: An Advanced in Situ Xrd Study. *J. Phys. Chem. C* **2011**, 115, 1506-1512.
27. vandeSandt, E. J. A. X.; Wiersma, A.; Makkee, M.; vanBekkum, H.; Moulijn, J. A., Catalyst Development for the Selective Hydrogenolysis of Ccl2f2 (Cfc-12) into Ch2f2 (Hfc-32). *Catal. Today* **1997**, 35, 163-170.
28. Tew, M. W.; Nachtegaal, M.; Janousch, M.; Huthwelker, T.; van Bokhoven, J. A., The Irreversible Formation of Palladium Carbide During Hydrogenation of 1-Pentyne over Silica-Supported Palladium Nanoparticles: In Situ Pd K and L-3 Edge Xas. *Phys. Chem. Chem. Phys.* **2012**, 14, 5761-5768.
29. Jin, M.; Liu, H.; Zhang, H.; Xie, Z.; Liu, J.; Xia, Y., Synthesis of Pd Nanocrystals Enclosed by 100 Facets and with Sizes <10 Nm for Application in Co Oxidation. *Nano Res.* **2011**, 4, 83-91.
30. Lim, B.; Jiang, M. J.; Tao, J.; Camargo, P. H. C.; Zhu, Y. M.; Xia, Y. N., Shape-Controlled Cynthesis of Pd Nanocrystals in Aqueous Solutions. *Adv. Funct. Mater.* **2009**, 19, 189-200.

31. Jin, M. S.; Zhang, H.; Xie, Z. X.; Xia, Y. N., Palladium Nanocrystals Enclosed by (100) and (111) Facets in Controlled Proportions and Their Catalytic Activities for Formic Acid Oxidation. *Energ. Environ. Sci.* **2012**, 5, 6352-6357.

32. Wojdyr, M., Fityk: A General-Purpose Peak Fitting Program. *J. Appl. Crystallogr.* **2010**, 43, 1126-1128.

33. Frisch, M. J.; Trucks, G. W.; Schlegel, H. B.; Scuseria, G. E.; Robb, M. A.; Cheeseman, J. R.; Scalmani, G.; Barone, V.; Mennucci, B.; Petersson, G. A., et al. Gaussian 09, Revision A.1. Gaussian Inc. Wallingford CT **2009**.

34. Lee, C. T.; Yang, W. T.; Parr, R. G., Development of the Colle-Salvetti Correlation-Energy Formula into a Functional of the Electron-Density. *Phys Rev B* **1988**, 37, 785-789.

35. Check, C. E.; Faust, T. O.; Bailey, J. M.; Wright, B. J.; Gilbert, T. M.; Sunderlin, L. S., Addition of Polarization and Diffuse Functions to the Lanl2dz Basis Set for P-Block Elements. *J. Phys. Chem. A* **2001**, 105, 8111-8116.

36. Soler, J. M.; Artacho, E.; Gale, J. D.; Garcia, A.; Junquera, J.; Ordejon, P.; Sanchez-Portal, D., The Siesta Method for Ab Initio Order-N Materials Simulation. *J. Phys.-Condens. Mat.* **2002**, 14, 2745-2779.

37. Dion, M.; Rydberg, H.; Schroder, E.; Langreth, D. C.; Lundqvist, B. I., Van Der Waals Density Functional for General Geometries. *Phys Rev Lett* **2004**, 92.

38. Zhang, H.; Jin, M.; Xiong, Y.; Lim, B.; Xia, Y., Shape-Controlled Synthesis of Pd Nanocrystals and Their Catalytic Applications. *Acc. Chem. Res.* **2012**.

39. Menegazzo, F.; Fantinel, T.; Signoretto, M.; Pinna, F., Metal Dispersion and Distribution in Pd-Based Pta Catalysts. *Catal. Commun.* **2007**, 8, 876-879.

40. Amorim, C.; Keane, M. A., Palladium Supported on Structured and Nonstructured Carbon: A Consideration of Pd Particle Size and the Nature of Reactive Hydrogen. *J. Colloid. Interf. Sci.* **2008**, 322, 196-208.
41. Ziemecki, S. B.; Jones, G. A.; Swartzfager, D. G.; Harlow, R. L., Formation of Interstitial Pd-C Phase by Interaction of Ethylene, Acetylene, and Carbon-Monoxide with Palladium. *J. Am. Chem. Soc.* **1985**, 107, 4547-4548.
42. Ziemecki, S. B.; Jones, G. A., Interstitial Carbon in Palladium. *J. Catal.* **1985**, 95, 621-622.
43. Maciejewski, M.; Baiker, A., Incorporation of Carbon into Palladium During Low-Temperature Disproportionation of Co over Pd/ZrO_2 Prepared from Glassy Pd-Zr Alloys. *J. Phys. Chem.* **1994**, 98, 285-290.
44. Han, Y. F.; Kumar, D.; Sivadinarayana, C.; Clearfield, A.; Goodman, D. W., The Formation of Pdcx over Pd-Based Catalysts in Vapor-Phase Vinyl Acetate Synthesis: Does a Pd-Au Alloy Catalyst Resist Carbide Formation? *Catal. Lett.* **2004**, 94, 131-134.
45. Crespo-Quesada, M.; Andanson, J.-M.; Yarulin, A.; Lim, B.; Xia, Y.; Kiwi-Minsker, L., Uv-Ozone Cleaning of Supported Poly(Vinylpyrrolidone)-Stabilized Palladium Nanocubes: Effect of Stabilizer Removal on Morphology and Catalytic Behavior. *Langmuir* **2011**, 27, 7909-7916.
46. Ormerod, R. M.; Lambert, R. M.; Bennett, D. W.; Tysoe, W. T., Temperature-Programmed Desorption of Coadsorbed Hydrogen and Acetylene on Pd(111). *Surf. Sci.* **1995**, 330, 1-10.
47. Azad, S.; Kaltchev, M.; Stacchiola, D.; Wu, G.; Tysoe, W. T., On the Reaction Pathway for the Hydrogenation of Acetylene and Vinylidene on Pd(111). *J. Phys. Chem. B* **2000**, 104, 3107-3115.

48. Andersin, J.; Lopez, N.; Honkala, K., Dft Study on the Complex Reaction Networks in the Conversion of Ethylene to Ethylidyne on Flat and Stepped Pd. *J. Phys. Chem. C* **2009**, 113, 8278-8286.

49. Torres, D.; Cinquini, F.; Sautet, P., Pressure and Temperature Effects on the Formation of a Pd/C Surface Carbide: Insights into the Role of Pd/C as a Selective Catalytic State for the Partial Hydrogenation of Acetylene. *J. Phys. Chem. C* **2013**, 117, 11059-11065.

50. Yang, B.; Burch, R.; Hardacre, C.; Headdock, G.; Hu, P., Influence of Surface Structures, Subsurface Carbon and Hydrogen, and Surface Alloying on the Activity and Selectivity of Acetylene Hydrogenation on Pd Surfaces: A Density Functional Theory Study. *J. Catal.* **2013**, 305, 264-276.

51. Van Hardeveld, R.; Hartog, F., Statistics of Surface Atoms and Surface Sites on Metal Crystals. *Surf. Sci.* **1969**, 15, 189-230.

SYNOPSIS TOC